Latin American Journal of Solids and Structures
www.lajss.org

Dynamic compressive and splitting tensile tests on mortar using split Hopkinson pressure bar technique

Abstract

Dynamic compressive and tensile properties of mortar under impact loading were investigated experimentally by using a split Hopkinson pressure bar (SHPB) apparatus with pulse shaping technique. Firstly, the basic principle, experimental limitations and some feasible improvements/modifications of SHPB technique used for dynamic tests on concrete-like materials were summarized briefly. And then the dynamic compressive strength, stress versus strain response, and failure modes of mortar were discussed and analyzed. Finally, a dynamic Brazilian disc test was conducted to obtain the splitting tensile property of mortar, and some typical experimental results were presented. Both compressive and splitting tensile results show that mortar is a strain-rate sensitive material. Either compressive or tensile strength enhances with the increase of strain rate, especially when the strain rate is greater than the transition strain rate, which is around 20 s^{-1} for the dynamic compression and 2.0 s^{-1} for the splitting tension, respectively. These findings are helpful to guide the design and application of concrete structures.

Keywords

Mortar; dynamic properties; SHPB; impact loading; splitting tension.

Fei Yang [a,c]
Hongwei Ma [a]
Lin Jing [b*]
Longmao Zhao [c]
Zhihua Wang [c]

[a] College of Science and Engineering, Jinan University, Guangzhou 510632,China
[b] State Key Laboratory of Traction Power, Southwest Jiaotong University, Chengdu, Sichuan 610031, China
[c] Institute of Applied Mechanics and Biomedical Engineering, Taiyuan University of Technology, 79 West Yingze Street, Taiyuan 030024, China

Corresponding author:
*jinglin_426@163.com

http://dx.doi.org/10.1590/1679-78251513

Received 15.08.2014
In revised form 23.10.2014
Accepted 30.10.2014
Available online 30.10.2014

1 INTRODUCTION

Mortar is a common type of concrete-like materials, and one of the most practical applications is used for rehabilitation and repair of reinforced concrete structures. These structures may be subjected to various dynamic loadings such as high-velocity impact, penetration and explosion. Therefore, understanding better the dynamic properties of concrete-like materials under various circumstances is a greatly significant issue for their engineering applications. It is well known that the mechanical behavior of concrete-like materials under dynamic loadings is strikingly different from that subjected to quasi-static loading conditions (Hughes, 1978; Grote, 2001; Ross, 1989).

Concrete-like materials are generally considered to be strain rate-sensitive. Both the tensile and compressive strengths increase with strain-rate, especially when the strain-rate is greater than a transition strain-rate, which is around 10^0 ~ 10^1 s^{-1} for the uniaxial tension and 10^2 s^{-1} for the uniaxial compression, respectively (Grote, 2001; Li, 2009; Ross, 1989; Wang, 2012). Dynamic increase factors (DIFs) are commonly used to describe the dynamic enhancements of concrete-like materials under high strain rate loadings. Based on a large number of dynamic compressive and tensile experimental results of concrete materials, Bischoff et al. (1991); Malvar et al. (1998) summarized and analyzed the quantitative relationship between DIF and strain rate, as shown in Figs. 1 and 2, respectively.

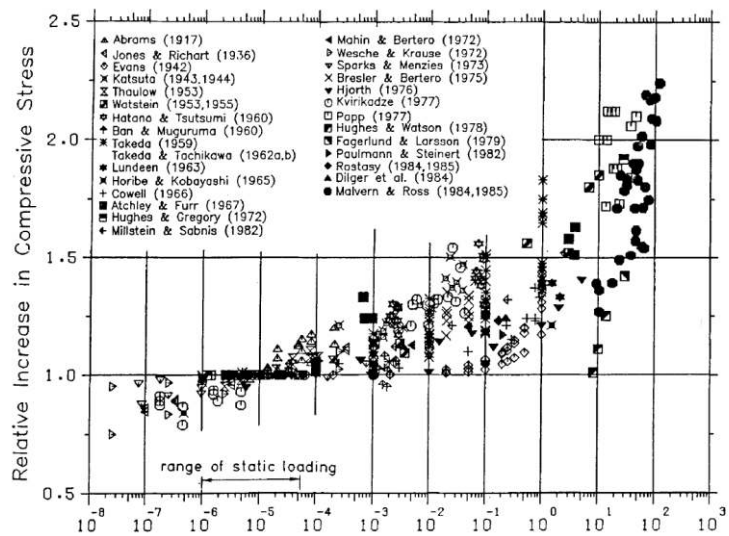

Figure 1: Effect of strain rate on the compressive strength of concrete (Bischoff, 1991).

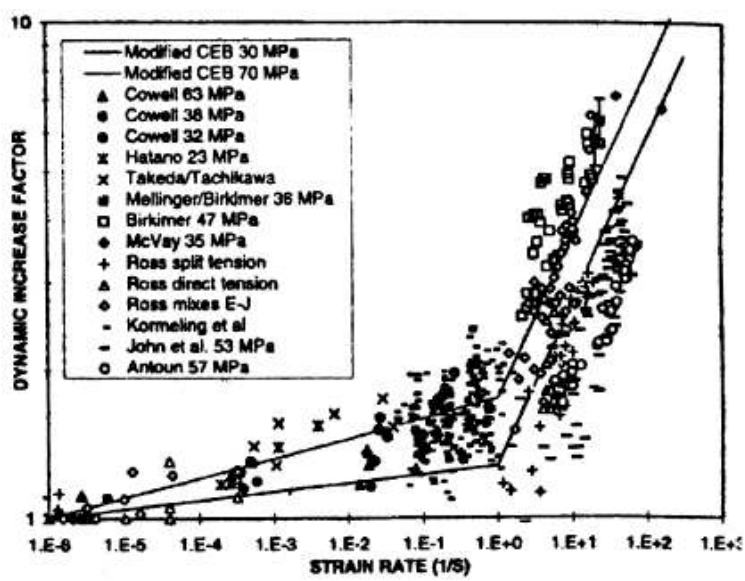

Figure 2: Effect of strain rate on the dynamic tensile strength (Malvar, 1998).

Split Hopkinson pressure bar technique, which decouples cleverly the inertia effect in structures and the strain rate effect in materials, has been used widely to characterize the dynamic compressive performance of various engineering materials at high strain rate in the region of 10^2 ~ 10^4 s^{-1} (Kolsky, 1949). With the use of large diameter Hopkinson bar to investigate the dynamic properties of concrete-like materials, some key problems such as high-frequency oscillation and dispersion of stress wave, and non-uniform stress/strain and non-constant strain rate deformation in the specimen, may be met in the tests (Gary, 1998; Zhao, 1998). In recent years, there has been increasing interest in employing pulse-shaping technique to determine the dynamic properties of concrete-like materials, aiming to attenuate high-frequency oscillations and increase the rise-time of the incident pulse, and achieve stress equilibrium and nearly constant strain-rate in the specimens (Chen, 2003; Duffy, 1971; Frew, 2002). Using the pulse-shaping SHPB apparatus, a large number of studies were conducted to investigate the dynamic mechanical properties of normal concrete (Zhang, 2009), high-strength concrete (Wang, 2012), and fiber-reinforced concrete (Li, 2009), and so on. However, few studies have been reported to investigate the dynamic response of mortar to impact loading, although it is significant for the engineering applications, as stated above.

In this study, the dynamic compressive and tensile tests on mortar were therefore conducted using a SHPB set-up with a pulse shaper, to assess and understand the dynamic response of mortar to impact loading.

2 SHPB TECHNIQUE FOR CONCRETE-LIKE MATERIAL TESTS

2.1 Basic principle

A typical SHPB test system generally consists of a striker (which is propelled by a gas gun), input bar, output bar, shock absorber and a data acquisition system, as shown in Fig. 3. With the impact of a striker at the free end of the input bar, a compressive longitudinal incident wave was created and then travels along the bar. When the stress wave reaches the specimen-bar interface, due to the mismatch of mechanical impedance between the specimen and pressure bar, it is partially reflected back into the input bar while the rest is transmitted into the output bar. The incident, reflected and transmitted pulse in the pressure bar were recorded by the resistance strain gauges attached to the input and output bar surface, respectively.

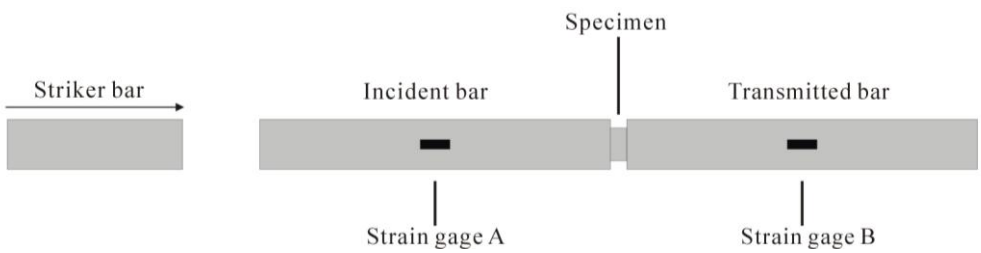

Figure 3: Schematic diagram of a typical SHPB apparatus.

Based on the one-dimensional elastic wave propagation theory, the stress, strain and strain rate of the specimen can be calculated by

$$\sigma_s = \frac{E_b A_b}{A_s} \varepsilon_t \tag{1}$$

$$\varepsilon_s = \frac{2c_0}{l_s} \int_0^t \varepsilon_r dt \tag{2}$$

$$\dot{\varepsilon}_s = \frac{2c_0}{l_s} \varepsilon_r \tag{3}$$

where E_b and A_b are the Young's modulus and cross-sectional area of the pressure bar, c_0 is the 1-D longitudinal elastic wave speed, A_s and l_s are the original cross-sectional area and length of the specimen, respectively.

2.2 Experimental limitations and improvements

2.2.1 Experimental limitations

A valid SHPB test is based on the following assumptions: (i) one-dimensional stress wave propagation in pressure bars; (ii) stress/strain uniformity within the specimen; and (iii) radial-inertia and friction effects of the specimen are negligible. For the SHPB tests of concrete-like materials, the brittle nature of materials and relatively large diameter of specimens and pressure bars, may result in violation of the above basic assumptions and affect the validity/accuracy of experiments.

Firstly, the small failure strain (less than 1%) of concrete-like materials often causes the specimen fail before stress uniformity within the specimen achieved, as a result of a sharp trapezoid-shaped incident wave in the conventional SHPB tests. Secondly, since concrete specimens are required to be large enough to contain sufficient micro-structures in order to be representative as a macroscopic "material test" (in the ASTM standard [2007], the minimum cross-sectional dimension of a rectangular section is at least three times the nominal maximum size of the coarse aggregate in the concrete specimen), the axial and radial inertia effects have greater influences on the actual stress-strain response of concrete-like materials. Radial inertia confinement may cause an apparent dynamic strength enhancement instead of the strain-rate sensitivity of the tested materials (Bischoff, 1991; Grote, 2001; Li, 2003). Thirdly, with the larger diameter of pressure bar, the stress wave propagation in the bars may not meet the one-dimensional wave assumption in nature; and 2-D effect caused by radial inertia become non-negligible, resulting in severe wave dispersion. Moreover, the experimental results are influenced by the complex boundary conditions (e.g. misalignment and interfacial friction at the bar-specimen surfaces), wave dispersion, specimen size effects on strength, and so on.

2.2.2 Improvements/modifications

To overcome these limitations and obtain the reliable experimental results, some feasible modifications have been developed and used in the SHPB tests for concrete-like materials. For example, the pulse-shaping technique was employed to increase the rising-time of incident wave, guaranteeing the reverberation times of the stress wave in the specimen is greater than 3 before the failure of the specimen, in order to achieve stress uniformity within the specimen.

Meanwhile, a theoretical optimal method for determining the length-to-diameter ratio of the SHPB specimen was modified by Samanta (1971) for metal materials to eliminate the effect of axial and radial inertia, where the material rate of change (i.e., the rate-of-change of a quantity that is defined with reference to specific particles of the moving continuum) was considered. He concluded that the influence of radial and longitudinal inertial stresses is the minimum for the small deformation specimens in the constant strain-rate SHPB tests, if the specimen dimension satisfying

$$\frac{l_s}{r} = \frac{\sqrt{3}}{4} \tag{4}$$

Similarly, Klepczko and Malinewski (1978) developed a modified formula for friction effect, that is,

$$\sigma = \sigma_0 \left(1 - \frac{2\mu r}{3l_s} \right) \tag{5}$$

where μ is the Coulomb friction coefficient, and the friction effects can be neglected for $2\mu r / 3l_s \ll 1$.

However, different from those metal materials (e.g. steel), concrete is hydrostatic – stress – dependent and the specimen size has great influence on its compressive/tensile strength. Zencker and Clos (1999) pointed out that the accurate dynamic stress versus strain curves can be obtained for the specimen with the slenderness ratio $l_s / d \leq 0.5$ in the one-dimensional stress state; and it can be also achieved for a relatively long specimen with $l_s / d \approx 1$ if both the 1-D stress state and uniformity of axial stress distribution are guaranteed. Therefore, an optional range $l_s / d = 0.5 \tilde{} 1.0$ is widely used in the tests.

3 DYNAMIC COMPRESSIVE TESTS

3.1 Experimental process

3.1.1 Specimens

The specimens were made of mortar which is a mixture of PO 42.5 cement, water and medium fine sand with average fineness modulus of 2.75. The mass radio of the three materials is 533:302:1600. The cylindrical SHPB specimens of diameter $D = 70$ mm and length $L = 55$ mm, and 100 x 100 x 100 mm cubic specimens and D75 x L150 cylinders for quasi-static tests were cast into the designed stainless steel moulds and placed into the conservation room for curing 28 days according to the technical standard. The quasi-static compressive strength of 100 mm cubes at an approximate strain rate of 10^{-3} s^{-1} is 28.7 MPa. The Young's modulus and Poisson's ratio determined from the standard tests on D75 x L150 mm cylinders are $E = 19$ GPa and $\mu = 0.13$, respectively. For the SHPB tests, the planeness of specimens was controlled below 0.02 mm to ensure the experimental precision.

3.1.2 Experimental set-up

The dynamic compressive tests of cement mortar samples were conducted using the conic variable cross-sectional SHPB with diameter of 74 mm. The lengths of the projectile, incident and transmitter bar, which are made of steel with Young's modulus equal to 200 GPa, are 800 mm, 3200 mm and 1800 mm, respectively. The sketch of the overall experimental set-up is shown in Fig. 4. Copper discs with diameter of 10 mm and thickness of 1.0 mm, which is with yield strength of 300 MPa, Young's modulus of 128 GPa and Tangent modulus of 1.28 GPa, were used as pulse shaper in the present study.

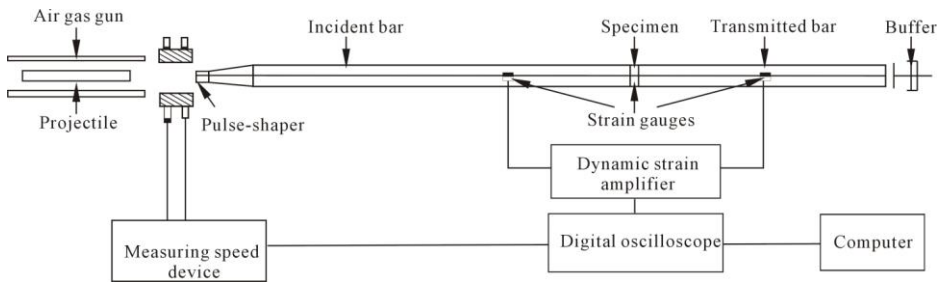

Figure 4: Sketch of the typical SHPB experimental set-up.

Two high dynamic strain amplifiers were used for calibration and to amplify the signals from the strain gauges. The original readings were acquired using a digital oscilloscope (TDS 420A, Tektronix.com, America). The impact velocity of the projectile, which is controlled by gas pressure, is measured by two parallel light gates and an electronic time counter. As described in Section 2.1, the incident, reflect and transmitted pulse in the pressure bar were recorded by the resistance strain gauges attached to the incident and transmitted bar surface, respectively. The dynamic compressive stress-strain relationship of specimens can be calculated using the recorded strain-time signals based on the one-dimensional stress wave theory.

3.2 Experimental Results

The dynamic compressive experiments of cement mortar samples were conducted at several different strain rates by using Split Hopkinson pressure bar with pulse-shaping technique. The details of the geometric dimension of specimens and pulse-shapers, experimental condition and results are listed in the Table 1.

3.2.1 Improvement on stress wave shape

The high-frequency oscillations of incident wave may cause large oscillations of stress-strain curve for the concrete-like materials with low strength and low Young's modulus, so that it is difficult to determine the upper and lower yield limits of tested materials. Moreover, the effects of dispersion and high-frequency oscillations of stress wave are evident for the dynamic test of non-homogeneous materials with large diameter Hopkinson bars. Pulse shaper was employed to expect to improve the stress wave shape, and therefore a comparison of stress wave generated with/without pulse shaper is made in this section.

Specimen number	Diameter (mm)	Length (mm)	Size of pulse-shaper (mm)	Rising-time of incident wave (μs)	$\dot{\varepsilon}$ (s^{-1})	f_{cd} (MPa)	Failure modes
1	70	53.24	-	61.1	29.3	47.6	No cracking
2	70	53.52	d 10× h 1.0	195.8	7.3	37.8	Edge-cracking
3	70	53.56	d 10× h 1.0	271.4	9.2	38.9	No cracking
4	70	52.93	d 10× h 1.0	291	15.7	47.1	Edge-cracking
5	70	54.26	d 10× h 1.0	266	24.5	46.7	Edge-cracking
6	70	52.50	d 10× h 1.0	208.2	25.2	43.7	No cracking
7	70	53.24	d 10× h 1.0	120	29.2	42.9	No cracking
8	70	51.87	d 10× h 1.0	183.9	32.1	57.3	Edge-cracking
9	70	53	d 10× h 1.0	179	36.7	54.5	Edge fracture
10	70	54.54	d 10× h 1.0	163.5	38.9	65.6	Edge-cracking
11	70	53.71	d 10× h 1.0	244	46.3	66.4	Hourglass-shape damage
12	70	53.05	d 10× h 1.0	196.1	51.7	80.1	Edge-cracking
13	70	53.49	d 10× h 1.0	217	53.6	75.5	Edge fracture
14	70	54.22	d 10× h 1.0	193	54.5	70.9	Hourglass-shape damage
15	70	53.64	d 10× h 1.0	162.5	60.2	79.6	Hourglass-shape damage
16	70	53.69	d 10× h 1.0	180	72.7	108.6	Hourglass-shape damage

Table 1: Dynamic compressive experimental result of mortar under different strain rates.

Fig. 5 shows the stress wave recorded by the strain gauge on the incident bar with/without pulse shaper. It is shown that a proper pulse shaper can attenuate high-frequency oscillations of incident stress wave to improve the stress wave shape. Usually, a nearly flat plateau in the reflected pulse in a SHPB test is used to judge the nearly constant strain rate in the specimen. It can be also found from Fig. 5 that the reflected wave could be improved to trend to generate a possible nearly flat plateau, as marked by the dotted rectangle. Surely, the achievement of pulse-shaping functions is highly dependent of a good matching between dynamic properties of the pulse-shaper material and the tested material and proper geometrical dimensions of the pulse-shaper for a given impact velocity.

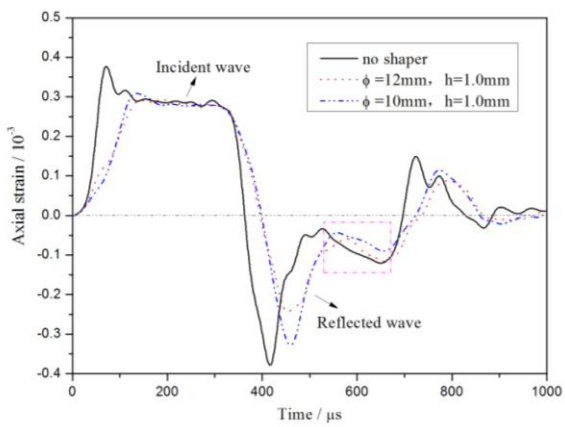

Figure 5: Stress wave shape with/without pulse shaper.

Another important function of the pulse shaper is to increase the rising-time of the incident pulse to facilitate stress equilibrium in the specimen. The rising-time of incident wave is the most important parameter for the validity assessment of stress equilibrium, which is closely related to the transit time t_0 required for the incident wave to travel a distance of the specimen length, given by

$$t_0 = l_s / c_s \tag{6}$$

where l_s and c_s are the specimen length and the longitudinal wave speed in the specimen, respectively. If the time duration required for the axial stress equilibrium within the specimen is τ, then the required reverberation times of the stress wave in the specimen is

$$n = \frac{\tau}{2t_0} \tag{7}$$

For a typical SHPB test for concrete-like materials, the stress uniformity state can be considered to achieve for $n \geq 3$ (Ravichandran, 1994). Therefore, to ensure the axial stress equilibrium within the specimen in an SHPB test, the rising-time of the incident pulse should be at least no less than τ, i.e.

$$t_r \geq \tau = 2nt_0 = \frac{2nL_s}{C_s} \tag{8}$$

In the present study, the longitudinal elastic wave speed, $c_s = \sqrt{E_s / \rho_s}$, for the tested mortar material is 2982 m/s, so the required values of the rising-time of incident wave should be greater than $6t_0$, that is, 110.7 μs for the specimen lengths of 55 mm. It can be found from Table 1 that all the rising-times of incident waves after using the pulse-shapers are greater than the required values tended to achieve axial stress equilibrium in the specimen.

3.2.2 Dynamic compressive strength

The dynamic stress-strain curves of specimens under different strain rates are shown in Fig. 6. It is found that cement mortar is a strain-rate sensitive material; both the uniaxial dynamic compressive strength and strain of specimens increase observably with the increase of strain rate. The peak strain of tested specimens seems to present an approximate increscent tendency with the rises of strain rate, although there is an abnormal peak strain for the specimen at the strain rate of 36.7 s^{-1}; this may be caused by the manufacture defect or experimental error.

As stated earlier, dynamic increase factor (DIF) is commonly used to describe the strain-rate effects on the compressive strength of brittle materials. The DIF values are calculated by

$$DIF = f_{cd} / f_{cs} \tag{9}$$

where f_{cd} and f_{cs} are the dynamic and quasi-static compressive strength of specimen, respectively. Fig. 7 gives the relationship between compressive DIF and strain rate in a semi-logarithmic form. It is obvious that the dynamic compressive strength of mortar enhances with the increase of

strain rate, especially when the strain rate exceeds ~20 s^{-1}; this strain rate is also named as transition strain rate. However, there is no consistent conclusion on the physical mechanism interpretation of the dynamic strength enhancement of concrete-like materials. The majority of researchers agree that such a strength increase is related with a materials viscosity due to the presence of free water in the pores of concrete at the low strain rate (Rossi, 1991; 1996). For the high strain rates, some authors believe it may attribute to be of structural origin (Ragueneau, 2003), which seems a non-homogeneous stress state within the specimen produced by inertia generates a large radial constraint similar with a confining pressure (Kotsovos, 1983). Others also explained this enhancement in strength is due to a delayed formation of the micro-cracks at increasing loading rate (Rossi, 1996).

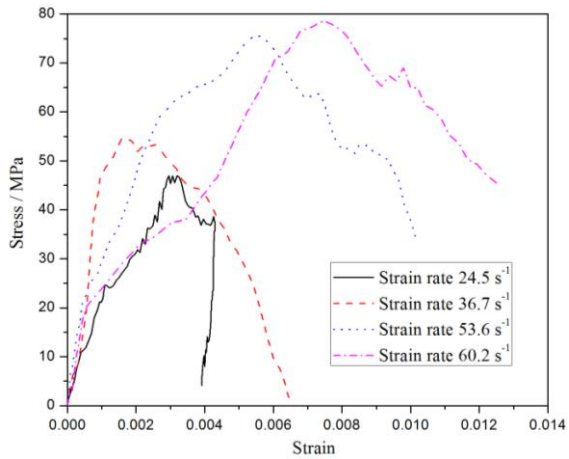

Figure 6: Stress-strain curves of cement mortar under different strain rates.

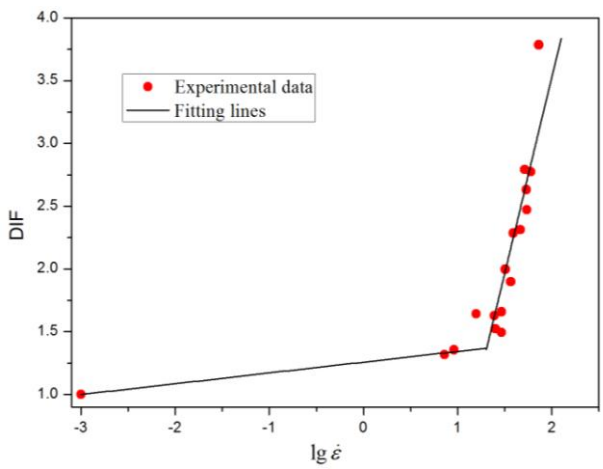

Figure 7: Relationship between compressive DIF of mortar and strain rate.

3.2.3 Dynamic failure modes

The impact failure modes of cement mortar specimens subjected to different strain rates are shown in Fig. 8. It can be observed from damage degree and fracture shape of samples that with the increase of strain rate, the damage of specimens accelerates and the number of fragments with

smaller size increases, respectively. Cement mortar specimens under quasi-static and low strain rates tend to axial split failure modes, while those often present "hourglass-shape" and shatter mode at higher strain rate. It should be pointed out that these failure modes of mortar specimens shown in Fig. 8 may be resulted by multiple pulses during the tests; the actual dynamic failure process and failure modes of specimens only subjected to single stress pulse loading, need to be investigated further by using high-speed camera.

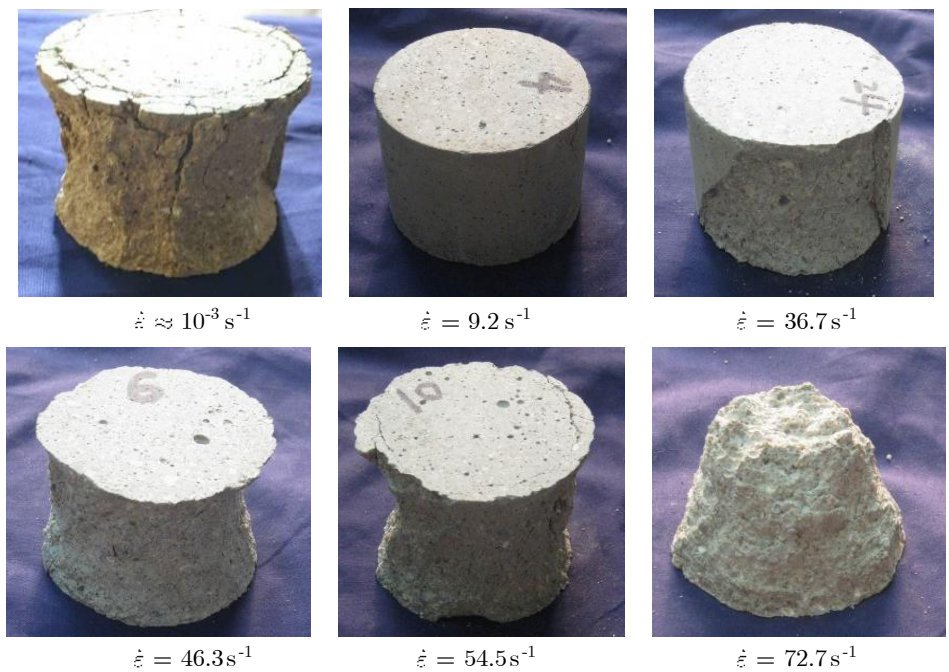

$\dot{\varepsilon} \approx 10^{-3}\,\mathrm{s}^{-1}$ $\dot{\varepsilon} = 9.2\,\mathrm{s}^{-1}$ $\dot{\varepsilon} = 36.7\,\mathrm{s}^{-1}$

$\dot{\varepsilon} = 46.3\,\mathrm{s}^{-1}$ $\dot{\varepsilon} = 54.5\,\mathrm{s}^{-1}$ $\dot{\varepsilon} = 72.7\,\mathrm{s}^{-1}$

Figure 8: Failure modes of cement mortar samples under different strain rates.

4 DYNAMIC TENSILE TESTS

Compared to compression, concrete-like materials are much weaker in tension (their tensile strength is 1/20 – 1/10 of the compressive value), which results that the failure of concrete-like materials often occurs via tension for the engineering structures. Therefore, understanding of the dynamic tensile properties of concrete-like materials is important for their applications. Usually, the dynamic properties of concrete-like materials can be measured using direct dynamic tensile tests (Reinhardt, 1982; Zielinski, 1982), dynamic bending tests (Tanaka, 1980), splitting (or Brazilian disc) tests (Lu, 2011; Neville, 1995) and spalling tests (Rong, 2012). In this study, the third method (i.e., Brazilian disc test) was adopted for mortar.

4.1 Fundamental theory

The Brazilian disc test is a simple indirect test method to measure the splitting strength of brittle materials. In this method, a thin circular disc is compressed along its diameter until it failures, as shown in Fig. 9. Based on elasticity theory, the stress distribution along the diametrical loading line of the disc specimen can be derived from the two-dimensional stress field, which is determined by the following equations (Neville, 1995; Timoshenko, 1951).

$$\sigma_x = \frac{2P}{\pi DL} \tag{10}$$

$$\sigma_y = \frac{2P}{\pi DL}\left|\frac{D^2}{y\ D-y} - 1\right| \tag{11}$$

where P is the force on the specimen at failure; D and L are the diameter and thickness of specimens, respectively; y is the ordinate of the point of interest in Fig. 9.

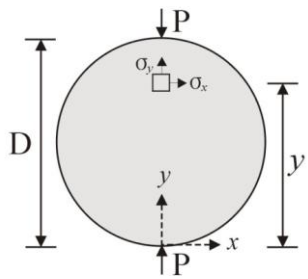

Figure 9: Schematic diagram of the Brazilian disc test.

In the dynamic Brazilian disc test using SHPB apparatus, if the dynamic stress equilibrium state is achieved, it is usually assumed that the engineering tensile stress near the center of the disc specimen is proportional to the peak value of the transmitted wave. So the dynamic tensile strength of specimens can be written in the quasi-static form:

$$\sigma_{td} = \frac{2P(t)}{\pi DL}, P(t) = \pi R^2 \sigma(t) \tag{12}$$

where σ_{td} is the dynamic tensile strength of specimens; P represents the force that is transmitted through the specimen; R is the radius of the pressure bar; $\sigma(t)$ is the peak stress of the transmitted wave.

Correspondingly, the strain rate in the specimen can be estimated by

$$\dot{\varepsilon} = \frac{\sigma_{td}}{E\tau} \tag{13}$$

where τ is the time lag between the start and the maximum of the transmitted stress wave, and E is Young's modulus of the specimen, where the static value is usually used for calculation due to the weak strain rate sensitivity.

In an actual test, the load is applied over a small zone, thus bearing strips are usually employed to control this zone and spread the load over the actual load-bearing width. ASTM (1986) recommends the width of the strips (w_0) should be approximately 1/12 of the diameter of the cylindrical specimen (d_s), a modified expression has been also proposed to estimate the tensile strength for a non-standard strip width test (Galvez, 2003), given by

$$\sigma_{td} = \frac{2P}{\pi l_s d_s}\left(1-\beta^2\right)^{3/2} \tag{14}$$

where $\beta = w_0/d_s$ is the relative width of the load-bearing strips.

4.2 Experimental arrangements

The dynamic Brazilian disc tests on mortar were conducted using the same SHPB apparatus as that in the compressive test, but with the different placement of specimens, as shown in Fig. 10. The dimension of specimens (diameter of 70 mm and thickness of 55 mm) is also the same. A pair of singly curved surface load-bearing strips with the width of 13 mm and thickness of 10 mm was used in the tests. Five strain gauges were mounted uniformly on the end-surface of specimens to explore the crack process, as shown in Fig. 11. Average quasi-static splitting tensile strength of D70 × L55 cylindrical mortar specimens with the same dimension and load-bearing strips is 4.7 MPa.

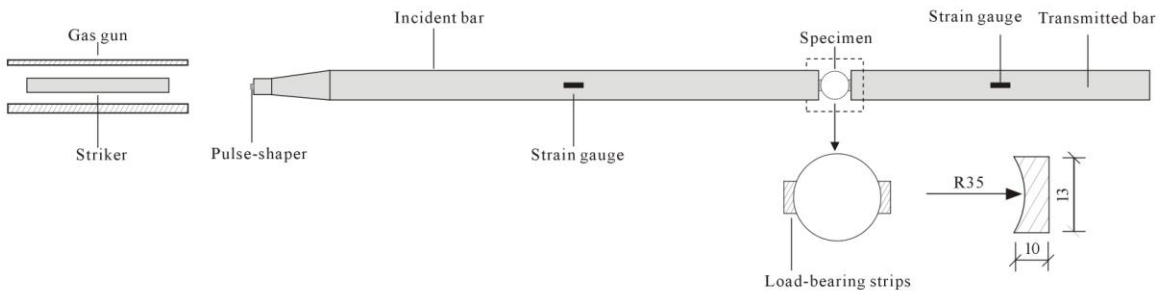

Figure 10: Schematic diagram of the dynamic Brazilian disc tests.

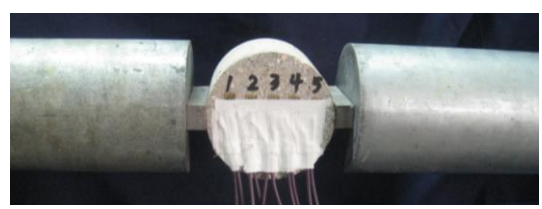

Figure 11: Photograph of the specimen mounted with strain gauges.

4.3 Experimental results

The information of specimens, experimental conditions and the corresponding test results are summarized in Table 2. The typical dynamic splitting failure modes, and dynamic splitting tensile strength of mortar determined from equation (14) are presented and discussed in the following subsections. Here, a typical stress history curve obtained from the specimen SP12 was shown in Fig. 12. It is clear that the dynamic stress response history is nearly linear during the whole loading process; the calculation of strain rate by using Eq. (13) is therefore considered to be accepted, although this method may be underestimated slightly the actual strain rate.

Specimen number	Diameter (mm)	Length (mm)	Size of pulse-shaper (mm)	Stress rate (GPa/s)	Strain rate (s^{-1})	Dynamic splitting strength (MPa)
SP1	70	53.20	-	35.91	1.89	5.0
SP2	70	54.05	-	111.53	5.87	9.3
SP3	70	54.73	-	88.54	4.66	7.2
SP4	70	53.29	-	38.76	2.04	5.1
SP5	70	53.37	-	74.29	3.91	6.9
SP6	70	53.54	-	66.69	3.51	6.2
SP7	70	51.78	-	66.31	3.49	6.2
SP8	70	53.05	-	56.05	2.95	5.6
SP9	70	54.49	d 10×h 0.8	18.43	0.97	4.8
SP10	70	54.44	d 10×h 0.8	20.9	1.10	4.75
SP11	70	52.48	d 10×h 0.8	59.85	3.15	6.9
SP12	70	54.25	d 10×h 0.8	69.16	3.64	7.0
SP13	70	53.09	d 10×h 0.8	85.5	4.5	7.1

Table 2: Dynamic splitting tensile experimental results of mortar.

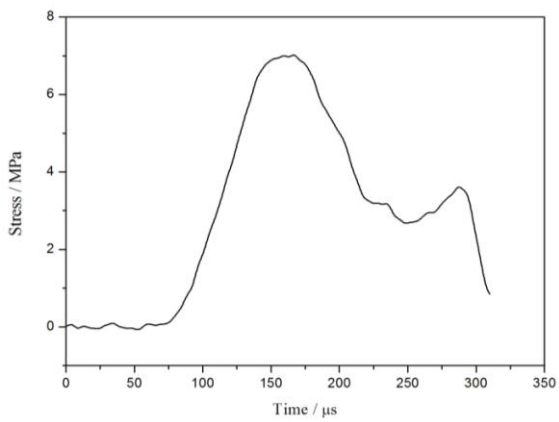

Figure 12: A typical stress history curve in the dynamic splitting tests.

4.3.1 Typical splitting failure modes

Fig. 13 shows the typical failure patterns of mortar specimens after dynamic splitting tests, compared to that under quasi-static test. It is shown that all the specimens split into two main halves along the loading path as expected. The damage degree of specimen under dynamic loading is more serious than that under quasi-static loading, and increases with the strain rate. In the dynamic case, with the major macro-crack develops, other cracks occur at the loading ends, resulting in the wedge-shaped local failure around the contact points. Two edge wedges of specimens are usually totally crushed into very small fragments at higher strain rate.

4.3.2 Dynamic splitting tensile strength

Similar to dynamic compressive tests, the tensile DIF was employed to describe the sensitivity of mortar to strain rate, as shown in Fig. 14. It is shown that the dynamic tensile strength also in-

creases with strain rate, where the transition strain rate is around 2.0 s^{-1}. Unlike the dynamic uniaxial compression, the dynamic tensile test is often considered as giving the "purest" information on mechanical behavior of concrete-like materials because the inertial effect does not reproduce a tensile strength (the inertia effects of traction produce a stress state close to a multiaxial state of traction) (Ragueneau, 2003). The dynamic strength enhancement in tension was may be attributed to the presence of free water and crack growth in concrete (Rossi, 1996).

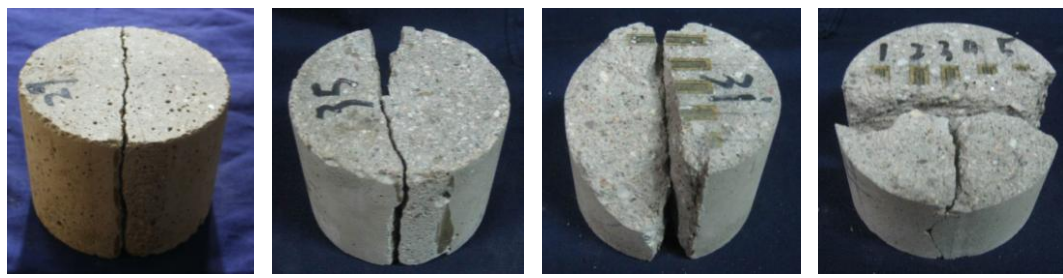

$\dot{\varepsilon} \approx 10^{-3}\,s^{-1}$ $\dot{\varepsilon} = 0.97\,s^{-1}$ $\dot{\varepsilon} = 3.64\,s^{-1}$ $\dot{\varepsilon} = 5.87\,s^{-1}$

Figure 13: Splitting failure patterns of mortar specimens.

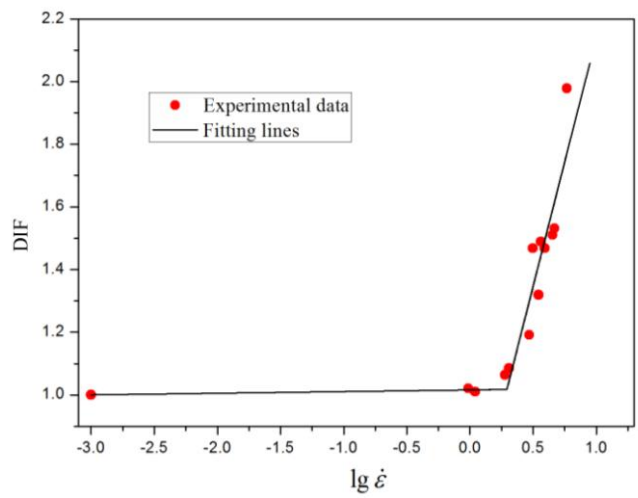

Figure 14: The quantitative relationship between tensile DIF and strain rate.

4.3.3 Crack growth process

As mentioned above, the crack growth may contribute to the dynamic tensile strength enhancement of mortar. This is because the micro-cracks propagating in the specimen needs more energy to initiate a new crack than to grow the old one, resulting that these cracks may be forced to propagate through the stronger fine aggregates rather than the weaker paste-aggregate interface. Therefore, it is interesting to explore the crack growth process of the dynamic splitting tensile specimens.

Fig. 15 shows a typical set of strain-time history curves of the specimen SP10 at strain rate of 4.75 s^{-1}. It can be found from Fig. 14 that the initial crack is observed at the approximate central

point of the disc specimen, as expected. Several micro-cracks along the loading path are formed at the early stage, and they develop separately with time but they assemble together later to become a main crack. According to the fracture time of two adjacent strain gauges, the velocities of crack growths can be estimated by dividing the length between these two strain gauges by the time interval. The values of the velocities calculated are 2916.7 m/s (for strain gauges 1 and 2), 804.6 m/s (for strain gauges 2 and 3), 1296.3 m/s (for strain gauges 3 and 4) and 2121.2 m/s (for strain gauges 4 and 5), respectively. An average velocity of the crack growth with the value of 1784.7 m/s is therefore obtained for the specimen SP10. It should be noted that, due to the irregularity of cracks, specimen defects, and the complexity of experimental conditions, the crack velocity obtained is only an approximate value; and a further and systematic study need to be conducted.

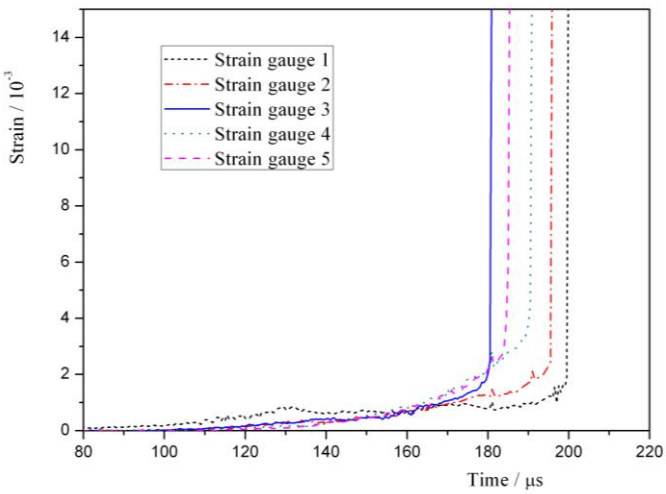

Figure 15: Typical strain-time history curves in tensile splitting tests (specimen SP10).

5 CONCLUSIONS

Dynamic compressive and splitting tensile tests on mortar under impact loading were conducted by using splitting Hopkinson bar technique with a pulse shaper. With regard to experimental limitations of SHPB tests on concrete-like materials, some feasible improvements and modifications were summarized. Results indicate that a proper pulse shaper can attenuate high-frequency oscillations of incident stress wave to improve the stress wave shape. Mortar is a strain-rate sensitive material; both compressive and tensile strength enhances with the increase of strain rate, especially when the strain rate is greater than the transition strain rate, which is around 20 s^{-1} for the dynamic compression and 2.0 s^{-1} for the splitting tension, respectively. An approximate crack velocity of 1784.7 m/s was obtained for the tested mortar at strain rate of 4.75 s^{-1}.

Acknowledgment

The authors wish to acknowledge the financial support provided by the China National Natural Science Funding (grant number 11390362) and opening foundation for State Key Laboratory of Explosion Science and Technology (grant number 33810005).

References

ASTM., (2007). Standard practice for making and curing concrete test specimens in the laboratory. ASTM C192/C192M.

ASTM., (1986). Standard test method for splitting tensile strength of cylindrical concrete specimens, ASTM C496-86, Annual book of standards. American Society for Testing Materials 256-259.

Bischoff, P.H., Perry, S.H., (1991). Compressive behaviour of concrete at high strain rates. Materials and structures 24(6): 425-450.

Chen, W., Song, B., Frew, D.J., Forrestal, M.J., (2003). Dynamic small strain measurements of a metal specimen with a split Hopkinson pressure bar. Experimental Mechanics 43(1): 20-23.

Duffy, J., Campbell, J.D., Hawley, R.H., (1971). On the use of a torsional split Hopkinson bar to study rate effects in 1100-0 aluminum. Transactions of the ASME, Journal of Applied Mechanics 37: 83-91.

Frew, D.J., Forrestal, M.J., Chen, W., (2002). Pulse shaping techniques for testing brittle materials with a split Hopkinson pressure bar. Experimental mechanics 42(1): 93-106.

Galvez, F., Galvez, V.S., (2003). Numerical modelling of SHPB splitting tests. J. Phys. IV 110:347-352.

Gary, G., Bailly, P., (1998). Behaviour of quasi-brittle material at high strain rate experiment and modelling. Eur. J. Mech., A/Solids 17(3): 403-420.

Grote, D.L., Park, S.W., Zhou, M., (2001). Dynamic behavior of concrete at high strain rates and pressures: I. experimental characterization. International Journal of Impact Engineering 25(9): 869-886.

Hughes, B.P., Watson, A.J., (1978). Compressive strength and ultimate strain of concrete under impact loading. Magazine of concrete research 30(105): 189-197.

Klepaczko, J., Malinowski, Z., (1978). Dynamic frictional effects as measured from the split Hopkinson pressure bar. In: Kawata, K., Shioiri, J., Editors. High velocity deformation of solids. Springer-Verlag Berlin.

Kolsky, H., (1949). An investigation of the mechanical properties of materials at very high rates of loading. Proceedings of the Physical Society. Section B 62(11): 676-700.

Kotsovos, M.D., (1983). Effect of testing techniques on the post-ultimate behaviour of concrete in compression. Materiaux et construction 16(1): 3-12.

Li, Q.M., Meng, H., (2003). About the dynamic strength enhancement of concrete-like materials in a split Hopkinson pressure bar test. International Journal of Solids and Structures 40: 343-360.

Li, W.M., Xu, J.Y., (2009). Impact characterization of basalt fiber reinforced geopolymeric concrete using a 100-mm-diameter split Hopkinson pressure bar. Materials Science and Engineering: A 513-514:145-153.

Lu, Y.B., Li, Q.M., (2011). About the dynamic uniaxial tensile strength of concrete-like materials. International journal of impact engineering 38(4): 171-180.

Malvar, L.J., Ross, C.A., (1998). Review of strain rate effects for concrete in tension. ACI Materials Journal 95(6): 735-739.

Neville, A.M., (1995). Properties of concrete, 4th edition. Harlow, England: Pearson Education Limited.

Ragueneau, F., Gatuingt, F., (2003). Inelastic behavior modelling of concrete in low and high strain rate dynamics. Computers and structures 81(12): 1287-1299.

Ravichandran, G., Subhash, G., (1994). Critical appraisal of limiting strain rates for compression testing of ceramics in a split Hopkinson pressure bar. Journal of the American Ceramic Society 77(1): 263-267.

Reinhardt, H.W., (1982). Concrete under impact loading, tensile strength and bond. Heron 27: 1-48.

Rong, Z.D., Sun, W., (2012). Experimental and numerical investigation on the dynamic tensile behavior of ultra-high performance cement based composites. Construction and Building Materials 31: 168-173.

Ross, C.A., Thompson, P.Y., Tedesco, J.W., (1989). Split-Hopkinson pressure bar tests on concrete and mortar in tension and compression. ACI Material Journal 86: 475-481.

Rossi, P., (1991). Influence of cracking in the presence of free water on the mechanical behaviour of concrete. Magazine of concrete research 43(154): 53-57.

Rossi, P., Toutlemonde, F., (1996). Effect of loading rate on the tensile behaviour of concrete: description of the physical mechanisms. Materials and structures 29(2): 116-118.

Samanta, S.K., (1971). Dynamic deformation of aluminium and copper at elevated temperatures. Journal of Mechanics and Physics of Solids, 19(3): 117-135.

Tanaka, K., Kagatsume, T., (1980). Impact bending test on steel at low temperatures. Bull. JSME 23:1736-1744.

Timoshenko, S., Goodier, J.N., (1951). Theory of elasticity, 2nd ed. McGraw-Hill, USA.

Wang, S.S., Zhang, M.H., Quek, S.T., (2012). Mechanical behavior of fiber-reinforced high-strength concrete subjected to high strain-rate compressive loading. Construction and Building Materials 31: 1-11.

Zencker, U., Clos, R., (1999). Limiting conditions for compression testing of flat specimens in the split Hopkinson pressure bar. Experimental mechanics 39(4): 343-348.

Zhang, M., Wu, H.J., Li, Q.M., et al., (2009). Further investigation on the dynamic compressive strength enhancement of concrete-like materials based on split Hopkinson pressure bar tests. Part I: Experiments. International journal of impact engineering 36: 1327-1334.

Zhao, H. (1998). A study on testing techniques for concrete-like materials under compressive impact loading. Cement and Concrete Composites 20(4): 293-299.

Zielinski, A.J., (1982). Fracture of concrete and mortar under uniaxial impact tensile loading. Doctoral thesis, Delft University of Technology: Netherland.